Article

Synthesis and characterization of a bi-directional photoswitchable antagonist toolbox for real-time GPCR photopharmacology

Niels J. Hauwert, Tamara A.M. Mocking, Daniel Da Costa Pereira, Albert J. Kooistra, Lisa M. Wijnen, Gerda Vreeker, Noortje W.E. Verweij, Bert H. De Boer, Martine J. Smit, Chris de Graaf, Henry F. Vischer, Iwan J. P. De Esch, Maikel Wijtmans, and Rob Leurs

J. Am. Chem. Soc., **Just Accepted Manuscript** • DOI: 10.1021/jacs.7b11422 • Publication Date (Web): 22 Feb 2018

Synthesis and characterization of a bi-directional photoswitchable antagonist toolbox for real-time GPCR photopharmacology

Niels J. Hauwert, Tamara A.M. Mocking, Daniel Da Costa Pereira, Albert J. Kooistra, Lisa M. Wijnen, Gerda C.M. Vreeker, Noortje W.E. Verweij, Bert H. de Boer, Martine J. Smit, Chris De Graaf, Henry F. Vischer, Iwan J.P. de Esch, Maikel Wijtmans*, Rob Leurs*

Email address: m.wijtmans@vu.nl, r.leurs@vu.nl

Division of Medicinal Chemistry, Amsterdam Institute for Molecules, Medicines and Systems, Faculty of Sciences, Vrije Universiteit Amsterdam, De Boelelaan 1108, 1081 HZ Amsterdam, The Netherlands

Abstract

Non-invasive methods to modulate G protein-coupled receptors (GPCRs) with temporal and spatial precision are in great demand. Photopharmacology uses photons to control *in situ* the biological properties of photoswitchable small-molecule ligands which bodes well for chemical biological precision approaches. Integrating the light-switchable configurational properties of an azobenzene into the ligand core, we developed a bi-directional antagonist toolbox for an archetypical family A GPCR, the histamine H_3 receptor (H_3R). From 16 newly synthesized photoswitchable compounds, VUF14738 (**28**) and VUF14862 (**33**) were selected as they swiftly and reversibly photoisomerize and show over 10-fold increased or decreased H_3R binding affinities, respectively, upon illumination at 360 nm. Both ligands combine long thermal half-lives with fast and high photochemical *trans*-/*cis* conversion, allowing their use in real-time electrophysiology experiments with oocytes to confirm dynamic photomodulation of H_3R activation in repeated second-scale cycles. VUF14738 and VUF14862 are robust and fatigue-resistant photoswitchable GPCR antagonists suitable for spatio-temporal studies of H_3R signaling.

Introduction

Optical control of biological processes is one of the emerging fields in biomedicine due to its high spatio-temporal resolution[1-5]. Initially, optogenetics revolutionized the field with major breakthroughs in e.g. the field of neuroscience[3]. Lately, the field of photopharmacology[1,2,5,6] has been providing a complementary framework allowing the use of photoswitchable ligand molecules to dynamically modulate native biological targets. In this framework, the photo-induced configuration of the ligand has either lower or higher affinity (directionality) than the 'dark' configuration, providing a means to reversibly regulate the biological target with light. It has very recently been applied to e.g. native membrane-bound ion channels[7-9] and G protein-coupled receptors (GPCR) [10-14]. Most GPCR examples have so far focused on single ligands typically incorporating a photosensitive group in the periphery of the GPCR ligands[10-14], successfully giving reversible mono-directional photoswitches. In this work, we present a bi-directional photoswitchable GPCR antagonist toolbox, i.e. a set of ligands from the same scaffold amenable to switching in two directions, showing either a light-induced increase or decrease in GPCR affinity, by positioning the photoswitchable moiety in the core of the new ligands.

To this end, we used a prototypic family A GPCR, the histamine H_3 receptor (H_3R). The H_3R is expressed mainly in the central nervous system (CNS) and involved in a variety of CNS processes[15-17]. Recently, the first H_3R antagonist (pitolisant, Wakix™) has been approved for the treatment of narcolepsy[18]. The medicinal chemistry of small-molecule H_3R ligands is well-developed[19,20] and provides interesting chemical opportunities to incorporate photoswitchable groups in order to obtain photoswitchable H_3R antagonists. The general H_3R antagonist pharmacophore includes a positively charged amine group[21], which is considered to interact with either the amino acid residues D114$^{3.32}$ or E206$^{5.46}$ in the transmembrane part of the H_3R protein[19,22,23]. A linker, usually an alkylether, allows the ligand to make a slight kink towards the bottom of the orthosteric H_3R binding site. The ether oxygen atom is connected to an aromatic core (e.g. phenyl, naphthyl, and many others[19,20]), which allows for π-π stacking interactions with aromatic H_3R residues, like the Y115$^{3.33}$, Y374$^{6.51}$, and F398$^{7.39}$ residues [24-26]. The aromatic core can be further substituted with a variety of groups including lipophilic groups, hydrogen bond acceptors, basic and acidic moieties.[27] Various photoswitchable moieties were evaluated for replacement of the H_3R antagonist aromatic core[5] and the photoisomerizable azobenzene moiety was deemed the best fit, because of the narrow, flat and elongated aromatic nature of its *trans* isomer. Although a naphthalene moiety has not been coined as an “azostere”[1], our design started from a

naphthalene-containing H_3R antagonist (**1**) developed by Roche et al.[28], which matches the previously mentioned pharmacophore criteria. We postulated that, due to the relatively small nature of the naphthalene core, additional room for π-π stacking interactions is present in the hydrophobic part of the H_3R binding site, allowing incorporation of the azobenzene photoswitch in the core of the H_3R scaffold (Fig. 1) itself rather than in the periphery, as most often observed for GPCR photo-ligands.

In this paper, we show how this core-centered strategy led to the new H_3R antagonists VUF14738 and VUF14862 that represent a bi-directional set of robust and fatigue-resistant photochemical GPCR antagonists and are unique assets to further detail H_3R pharmacology. We envision that these ligands are useful molecular tools for e.g. probing H_3R mediated responses in physiology in a similar fashion as stereoisomers like R- and S-α-methylhistamine[29,30], but having control of H_3R affinity using an external trigger. Moreover, in view of the importance of the H_3R in various brain functions[17,31], spatiotemporal photopharmacology approaches will bring new experimental options (next to optogenetics) in order to delineate the importance of local neuronal circuits in H_3R pharmacology.

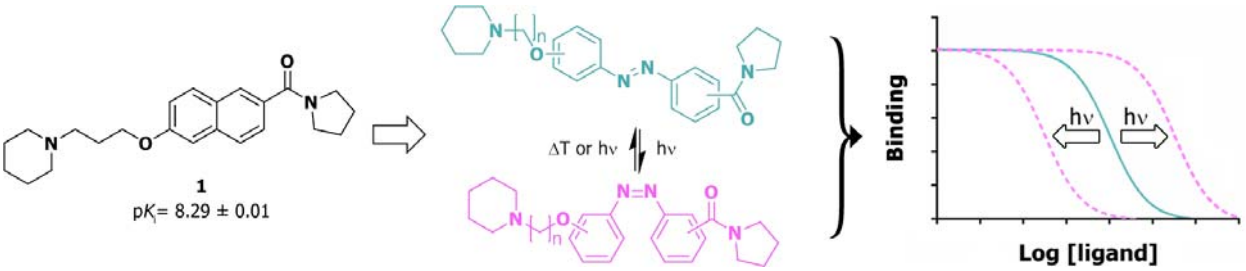

Figure 1: General design and concept of bi-directional photoswitchable H_3R antagonists. In this SAR study, the azobenzene moiety is incorporated in the core of compound 1 to give a series of differently substituted *trans* isomers (cyan). Illumination leads to their corresponding *cis* isomers (magenta). Within this study, we aimed to discover photoswitchable H_3R antagonists that show at least a 10-fold increase or decrease in GPCR affinity upon illumination.

Results & Discussion

Synthesis and photochemical characterization of azobenzene-derived H_3 ligands

Three synthesis routes were developed which allowed for great versatility in the substitution patterns of the azobenzene moiety (Scheme 1). A set of anilines was obtained by an amide coupling from **2**-**4** to **5**-**7**. The anilines underwent diazotization followed by a quench with phenol to afford **8**-**11** and Williamson ether synthesis to yield the *para*-ether substituted H_3R photoswitchable ligands **12**-**17**.

The second route was designed to overcome the undesired *para*-selectivity in the diazotization and comprises oxidation of aniline **18** and **19** to a nitroso-intermediate, condensation with an aniline to furnish **20**-**24** and a Pd/RockPhos-catalyzed ether synthesis[32] to yield *meta*-ether substituted ligands **25**-**30**. For the synthesis of constrained ligands, either a Mitsunobu reaction (for **31** and **33**) or a Pd/RockPhos-catalyzed ether synthesis[32] (for **32**) was employed instead of the Williamson ether synthesis. The Mitsunobu approach was unable to yield **34** and instead a tosylate-displacement strategy was used for this compound.[33]

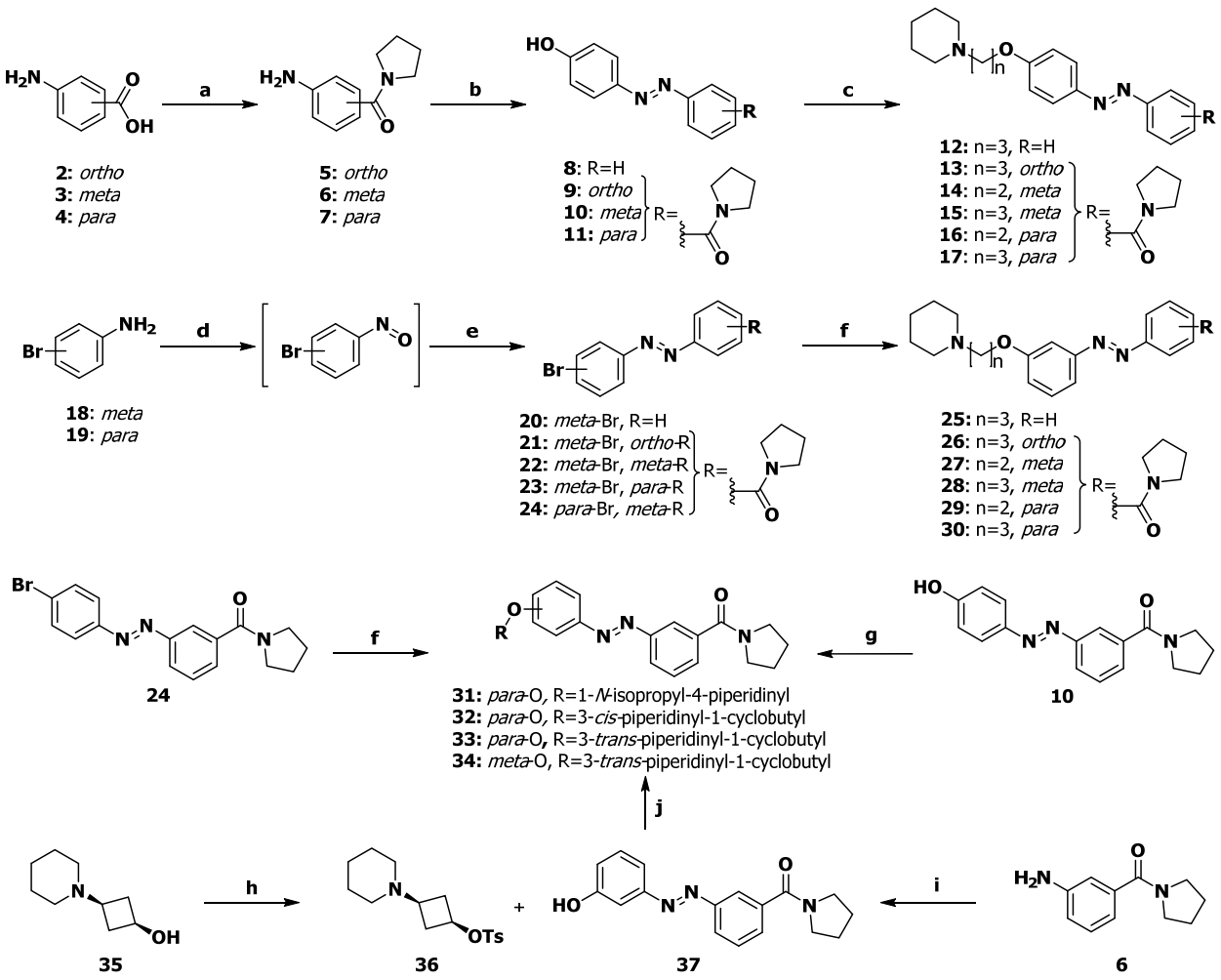

Scheme 1: General synthetic scheme for photoswitchable H_3R antagonists. Reagents and conditions: (a) pyrrolidine, EDCI.HCl, DIPEA, HOBt.H_2O, DMF, RT, 16 hrs, 57 – 95%; (b) (I) $NaNO_2$, 1M aq. HCl, 0°C, 5 min; (II) phenol, aq. NaOH, RT, 30 min; (III) 1M aq. HCl, aq. sat. NH_4Cl, RT, 10 min, 30 – 81%; (c) NaI, K_2CO_3, Pip-$(CH_2)_n$-Cl.HCl, DMF, 130°C, 16 hrs, 31 – 76%; (d) Oxone™, H_2O:DCM 4:1, RT, 3 hrs; (e) R-Ar-NH_2, AcOH:DCM 1:1, RT, 16 hrs, 30 – 76% (over 2 steps); (f) R-OH, RockPhos, $[PdCl(C_3H_5)]_2$, Cs_2CO_3, PhMe, 90°C, 23 hrs, 12 – 47%; (g) R-OH, DEAD, PPh_3, THF, 0°C→ RT, 18 hrs, 73 – 33%; (h) 1-methylimidazole, 4-Me$PhSO_2Cl$, DCM, RT, 48 hrs, 43%; (i) (I) Oxone™, H_2O:DCM 4:1, RT, 6 hrs; (II) 3-OTBMDS-aniline, AcOH, RT, 16 hrs; (III) TBAF, THF, 0°C, 10 min, 13%; (j) (I) NaH, DMF, RT, 30 min; (II) 36, 90 °C, 16 hrs, 59%; Pip=1-piperidino.

We first investigated the photoisomerization of all final compounds as well as their thermal relaxation at 20 °C as determined by the method of Priimagi *et al*[34] (Table 1, Fig. S1). Clear trends in the photochemistry could be deduced. It was observed that *para*-ether derivatives (scaffold A) have a distinctly higher λ_{max} for the π-π^* transition of the *trans* isomers than *meta*-ether derivatives (scaffold B). This trend can be explained due to a better "push-pull" profile in the electron density of the

azobenzene unit of scaffold A, which is known to red shift the λ_{max} of electronic transitions[35,36]. It was found that upon continuous illumination at 10 mM in DMSO-d_6 with 360 ± 25 nm light a photostationary state (PSS) containing over 85% *cis* isomer (LC area at 254 nm) could be obtained for all compounds, with several ligands showing a PSS containing more than 95% *cis* isomer.

Various trends can be observed regarding the thermal relaxation half-lives of the compounds. In line with literature, we observed a 3 to 5-fold difference in thermal relaxation half-life between the *para*-ethers (**12**, **13**, **15**, **17**) and their respective *meta*-ether (**25**, **26**, **28**, **30**) analogs having a propyl-piperidine side chain.[37] Such an effect can be attributed to increased conjugation in the *para*-derivatives[38]. In the series of ethyl-piperidine analogs (**14** *versus* **27**, **16** *versus* **29**) this effect of *para*- versus *meta*-ether substitution is even more pronounced, increasing the differences in thermal relaxation half-life to 360 and 212-fold, respectively. The propyl, cyclobutyl and 4-piperidinyl spacers appear to have a comparable influence on the thermal relaxation half-lives (compare **15** versus **31-33**, and **15/28** *versus* **33/34**). If the amide group is placed at the *ortho* (**13**, **26**) or *para* position (**17**, **30**) the thermal relaxation half-life is comparable to its non-substituted counterpart (**12**, **25**). However, having the amide in the *meta* position as in **15/28** yields a modest increase in thermal relaxation half-life[39].

Table 1: Structure-photochemistry relationship of the photoswitchable antagonist series.

		A					B
		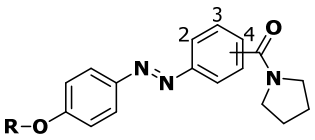					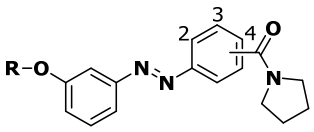
Compound Number	**Scaffold**	**R**	**Amide position**	**λ_{max} *trans* (nm)**	**λ_{max} *cis* (nm)**	**$t_{½}$ @ 20 °C (days)[b]**	**PSS[a] ± SEM (area % *cis*)**
12	**A**	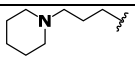	**-[c]**	**344**	**432**	**11.2**	**96.6 ± 0.33**
25	**B**	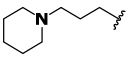	**-[c]**	**317**	**430**	**52.2**	**93.2 ± 0.29**
17	**A**	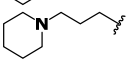	**4**	**352**	**435**	**9.52**	**88.2 ± 2.5**
30	**B**	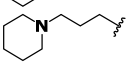	**4**	**323**	**431**	**29.3**	**88.9 ± 1.3**
16	**A**	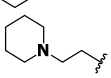	**4**	**349**	**434**	**0.23**	**86.6 ± 2.5**
29	**B**	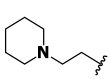	**4**	**324**	**429**	**48.8**	**91.3 ± 1.4**
15	**A**	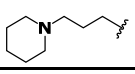	**3**	**347**	**432**	**26.5**	**95.4 ± 0.50**

28	**B**	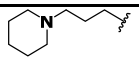	**3**	**318**	**427**	**122**	**86.8 ± 0.63**
14	**A**	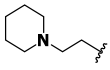	**3**	**345**	**431**	**0.69**	**90.6 ± 0.77**
27	**B**	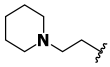	**3**	**318**	**425**	**248**	**89.3 ± 0.50**
13	**A**	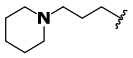	**2**	**351**	**430**	**10.9**	**88.9 ± 2.2**
26	**B**	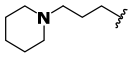	**2**	**321**	**428**	**48.8**	**88.4 ± 1.8**
31	**A**	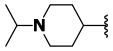	**3**	**346**	**434**	**33.5**	**90.5 ± 1.3**
32	**A**	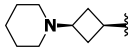	**3**	**346**	**431**	**27.0**	**96.8 ± 0.21**
33	**A**	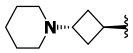	**3**	**346**	**432**	**29.2**	**94.6 ± 1.8**
34	**B**	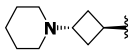	**3**	**317**	**425**	**161**	**89.3 ± 0.40**

[a]Photostationary state area percentages after illumination at 10 mM in DMSO-d_6 and as determined by LCMS analysis at 254 nm. [b]Thermal relaxation half-life times were determined according to the method of Priimagi *et al.*[34] Arrhenius plots are available in Fig. S1 [c]Unsubstituted phenyl moiety.

Compounds **28** and **33** were selected for further photochemical characterization based on their favorable pharmacological characteristics (*vide infra*). The thermal relaxation half-life times for these compounds in 50 mM Tris-HCl pH 7.4 buffer at room temperature were also directly determined, resulting in half-lives of 114 days for compound **28** (Fig. S2) and 26 days for compound **33** (Fig. S3). These long thermal relaxation half-lives are similar to the values obtained from the Arrhenius plots at 20 °C and uniquely allowed for a thorough analysis of the photoswitching and relaxation process by ^{1}H-NMR spectroscopy in conjunction with LC-MS chromatography and UV-Vis spectroscopy. We first investigated isomerization of **28** and **33** at 10 mM in DMSO-d_6 by monitoring both ^{1}H-NMR and LC-MS profiles in time. While multiple ^{1}H-NMR signals change upon photoswitching, the signals for the CH or CH_2 group adjacent to the ether O-atom provided a clearly resolved signal for quantification (Fig. 2A, C). For both **28** and **33** the percentages of isomerization as analyzed by ^{1}H-NMR spectroscopy and LC-MS analysis at 254 nm (Fig. 2B, D) are comparable yet slightly different, reflecting most likely some differences in ε-values of the *trans* and *cis* isomers (Table S1). Despite these minor differences, LC-MS was subsequently used as a routine analysis in view of the higher throughput.

Next, the photoisomerization rate was investigated at 25 μM in 50 mM Tris-HCl pH 7.4 buffer supplemented with 1% DMSO-d_6 using UV-Vis spectroscopy (Fig. 2E, F). Rapid photoisomerization was observed for both compounds during illuminations at both 360 ± 25 nm and 430 ± 17 nm to obtain high amounts of *cis* isomer or considerable amounts of *trans* isomer, respectively (Fig. S4-S6, S10-S12). After

30 seconds of illumination, isomerization of both key compounds had reached isomerization percentages within 5% of their PSS. Thus, illuminating for 300 seconds was always sufficient to reach PSS. Arguably due to both solvent and concentration effects[36,40,41] the measured isomerization rates are considerably higher in the experiments performed at 25 μM in buffer, compared to the measurements at 10 mM in DMSO-d_6 of the two H_3R ligands.

We subsequently studied the real-time isomerization behavior of both compounds at a concentration of 25 μM in 50 mM Tris-HCl pH 7.4 buffer supplemented with 1% DMSO-d_6 using a setup which allowed the illumination perpendicular to the path of the UV-Vis spectrometer light source. Under these conditions, we determined a photoisomerization half-life for **33** of 4 ± 0.2 seconds under illumination with 360 ± 25 nm and 8 ± 0.6 seconds under illumination with 430 ± 17 nm (Fig. 2G). For **28** the values were found to be 16 ± 0.9 seconds under illumination at 360 ± 25 nm and 11 ± 0.3 seconds under illumination at 430 ± 17 nm (Fig. 2H).

Both photoswitchable compounds proved to be very photostable. Even after 48 hours of illumination at 360 ± 25 nm with an intensity of 0.77 mW/mm^2 no apparent photodegradation was visible in both ^{1}H-NMR and LC-MS analyses of **28** and **33**. To exemplify the resistance to fatigue of **28** and **33** over 1000 isomerization cycles switching between illumination at 360 ± 25 and 430 ± 17 nm with 20-second intervals were executed. The absorbance at λ_{max} of the π-π* transition of the *trans* isomer did not alter considerably (Fig. 2I, 2J, S16 and S17) indicating that both key photoswitches are highly resistant to photobleaching.

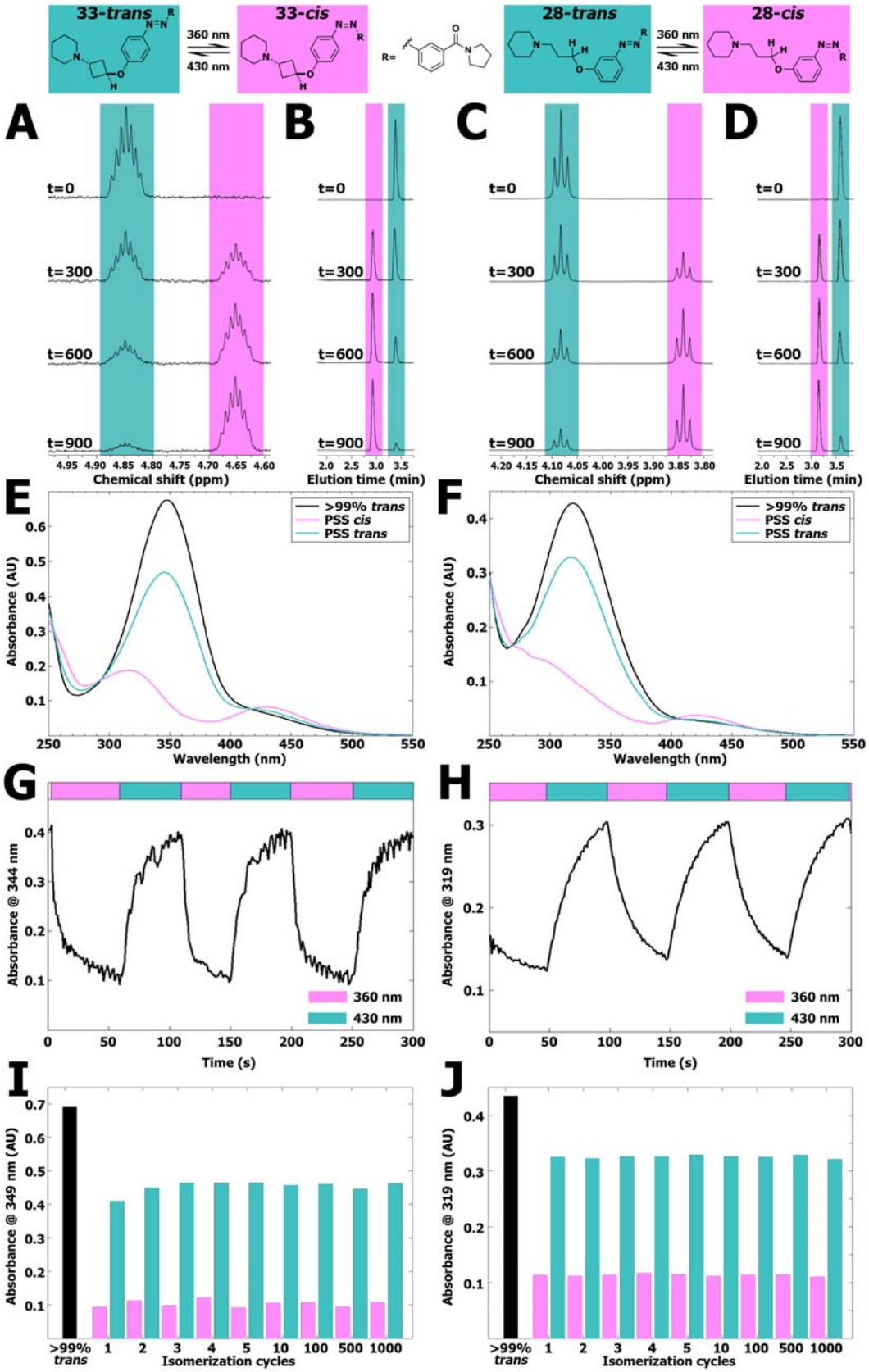
33-trans
360 nm
430 nm
33-cis
R=
28-trans
360 nm
430 nm
28-cis
A
B
C
D
t=0
t=300
t=600
t=900
Chemical shift (ppm)
Elution time (min)
E
F
>99% trans
PSS cis
PSS trans
Absorbance (AU)
Wavelength (nm)
G
H
Absorbance @ 344 nm
Absorbance @ 319 nm
360 nm
430 nm
Time (s)
I
J
Absorbance @ 349 nm (AU)
Absorbance @ 319 nm (AU)
>99% trans
1
2
3
4
5
10
100
500
1000
Isomerization cycles

Figure 2: (A) A representative part of ^{1}H-NMR spectra of 10 mM of compound 33 in DMSO-d_6 illuminated at 360 ± 25 nm displayed at various time points (seconds). The presented peak belongs to the hydrogen atom explicitly drawn in the structure shown above the spectrum. The full ^{1}H-NMR spectra are available in supplementary figure S18. (B) A representative part of LC-MS chromatograms belonging to the illuminated NMR samples shown in Fig. 2A. The full chromatograms are available in supplementary figure S19. (C) A representative part of ^{1}H-NMR spectra of 10 mM of compound 28 in DMSO-d_6 illuminated at 360 ± 25 nm displayed at various time points (seconds). The presented peak belongs to the hydrogen atom explicitly drawn in the structure shown above the spectrum. The full ^{1}H-NMR spectra are available in supplementary figure S20. (D) A representative part of LC-MS chromatograms belonging to the illuminated NMR samples shown in Fig. 2C. The full chromatograms are available in supplementary figure S21. (E) UV-Vis spectra of 25 μM of compound 33 (*trans*) in 50 mM Tris-HCl pH 7.4 buffer containing 1% DMSO-d_6. PSS *cis* represents a sample which has been illuminated for 300 seconds using 360 ± 25 nm light. PSS *trans* represents subsequent illumination for 300 seconds using 430 ± 17 nm. (F) UV-Vis spectra of 25 μM of compound 28 (*trans*) in 50 mM Tris-HCl pH 7.4 buffer containing 1% DMSO-d_6. PSS *cis* represents a sample which has been illuminated for 300 seconds using 360 ± 25 nm. PSS *trans* represents subsequent illumination for 300 seconds using 430 ± 17 nm. (G) Absorbance at 344 nm of 25 μM of compound 33 in 50 mM Tris-HCl pH 7.4 buffer + 1% DMSO-d_6. UV-Vis spectra were obtained with 1-second intervals under alternating illumination with 360 ± 25 nm and 430 ± 17 nm perpendicular to the light source of the UV-Vis spectrometer. (H) Absorbance at 319 nm of 25 μM of compound 28 in 50 mM Tris-HCl pH 7.4 buffer + 1% DMSO-d_6. UV-Vis spectra were obtained with 1-second intervals under alternating illumination with 360 ± 25 nm and 430 ± 17 nm perpendicular to the light source of the UV-Vis spectrometer. (I) Repeated isomerization cycles of 25 μM of compound 33 in a pH 7.4 buffer containing 15 mM HEPES, 64 mM NaCl, 25 mM KCl, 0.4 mM $CaCl_2$ and 0.8 mM $MgCl_2$ containing 1% DMSO-d_6 analyzed at 349 nm. PSS *cis* was obtained by using illuminations for 20 seconds at 360 ± 25 nm. PSS *trans* was obtained by using illuminations for 20 seconds at 430 ± 17 nm. An extended figure is available in supplementary figure S16. (J) Repeated isomerization cycles of 25 μM of compound 28 in a pH 7.4 buffer containing 15 mM HEPES, 64 mM NaCl, 25 mM KCl, 0.4 mM $CaCl_2$ and 0.8 mM $MgCl_2$ containing 1% DMSO-d_6 analyzed at 319 nm. PSS *cis* was obtained by using illuminations for 20 seconds at 360 ± 25 nm. PSS *trans* was obtained by using illuminations for 20 seconds at 430 ± 17 nm. An extended figure is available in supplementary figure S17.

Photopharmacological characterization

Because of their long thermal relaxation half-lives, the newly synthesized photoswitchable GPCR ligands are uniquely compatible with competition radioligand-binding experiments. All new azobenzene-derived H_3R ligands, either illuminated using 360 ± 25 nm to PSS (as determined by LC-MS) or kept in the dark, were evaluated for their affinity for the human H_3R by a [^{3}H]-N$^{\alpha}$-methylhistamine competition binding experiments performed in the dark. Both histamine and, as previously reported[28], the parent naphthalene-compound **1** potently displace [^{3}H]-N$^{\alpha}$-methylhistamine binding to membranes overexpressing the H_3R (Table 2) and their affinity values were not affected by illumination of the compound solutions at 360 ± 25 nm (data not shown). Replacement of the naphthalene core of **1** with the azobenzene core resulted in a series of moderate to highly potent H_3R ligands with pK_i values

between 6.01 and 8.76 as *trans* isomers (i.e. without illumination). The direct azobenzene analog of **1**, compound **17**, bound the H_3R with only a slightly lower affinity (pK_i = 7.96 ± 0.06, Table 2) compared to **1** (pK_i = 8.29 ± 0.01, Table 2). Furthermore, the affinity for H_3R was modulated effectively by shifting the position of the amine side chain, with scaffold A (*para*-substitution) always resulting in better affinities than scaffold B (*meta*-substitution) (Table 2). In general, the propyl spacer proved advantageous over the ethyl spacer for H_3R affinity. The effects of amide positioning varied amongst the different subclasses.

Rather than absolute affinities of the *trans* isomers for H_3R, the shift in affinity upon illumination was considered the prime parameter for photopharmacology applications and selection of key compounds. An increase in binding affinity upon photoisomerization (illumination at 360 ± 25 nm) was observed for **12**, **25**, **27**, **28** and **30**. Interestingly, most of these compounds contain a *meta*-ether-substituted azobenzene core (scaffold B) with either a 3-carboxamide (**27**, **28**), a 4-carboxamide (**30**) or no carboxamide substituent (**25**). The ethyl-spaced **27** has an 8.3-fold decrease in H_3R affinity compared to the propyl-spaced analog **28**. Within the set of compounds lacking a carboxamide, *meta*- and *para*-ether-substituted azobenzene compounds **25** and **12** (scaffolds B and A) show similar shifts in H_3R affinity upon isomerization. The 13.5-fold increase in H_3R affinity upon photoswitching of **28** (Fig. 3A) led to its identification as one of the key compounds of this study (VUF14738).

Compounds that show decreased H_3R binding affinity upon isomerization were primarily found to have a *para*-ether-substituted azobenzene (scaffold A). The trend that ethyl-spaced compounds perform less well than their respective propyl-spaced analogs was also observed for the pairs **14**/**15** and **16**/**17**. Derivatives with a 2-carboxamide substituents (**13**, **26**) gave smaller shifts in H_3R affinity compared to their 3-carboxamide counterparts (**15**, **28**). The observed decreases in H_3R binding affinity upon isomerization observed for these compounds (**13-17**, **26** and **29**) were deemed insufficient for proper photopharmacological application. To address this issue, the core azobenzene-substituted scaffold was maintained but the propyl spacer between the ether and piperidine moiety was constrained using isopropylpiperidinyl and 1,3-cyclobutyl spacers. Such linker rigidification is a known strategy to increase the binding affinity of H_3R antagonists[33,42]. Importantly, we reasoned that the limited degrees of freedom associated with the linker rigidification would hamper the *cis* isomer from (partially) readjusting its binding mode in the GPCR protein. Upon linker rigidification, the H_3R binding affinities for **31** and **33** were considerably increased compared to their flexible counterpart **15** (Table 2). Additionally, a pronounced increase in the shift in H_3R affinity between the *trans* and *cis* analogs was

observed. Of note is the lower H_3R affinity of stereoisomer **32** compared to **33**, which is in accordance with previously reported data[33]. Compound **33** outperformed **31** based on having a larger shift in H_3R affinity (11.2-fold lower, Fig. 3B) upon isomerization and higher absolute H_3R affinity. Moving the *trans*-cyclobutyl side-chain to the *meta*-position (**34**), effectively arriving at a constrained version of key compound **28**, virtually abolished the pK_i shift and did not increase the binding affinity. All this led to the designation of **33** as second key compound (VUF14862).

Compounds **28** and **33** either gain or lose at least 10-fold H_3R affinity upon illumination (Fig. 3A, B). Thus, using the same photoswitchable core and by proper side chain substitution in the periphery of the scaffold, we developed bi-directional GPCR photoswitchable ligands. Moreover, **28** and **33** show a 10 to 100-fold H_3R selectivity over the H_1R and no measurable affinity for H_2R and H_4R (Table S2). With the cautious use of **28** in view of its residual H_1R affinity**, 28** and **33** offer a bi-directional set of photopharmacological tools for H_3R.

Table 2: Affinity for the human H_3R of photoswitchable azobenzene-derived H_3R ligands

		A		B				
		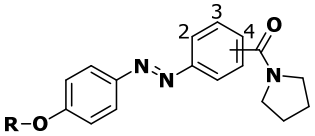		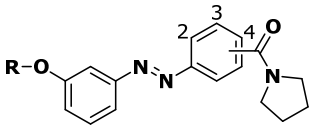				
Compound number	**Scaffold**	**R**	**Amide position**	**PSS[a] ± SEM (area % *cis*)**	**pK_i *trans* ± SEM[b]**	**pK_i at PSS[a] ± SEM[b]**	**pK_i shift[c]**	**n**
Histamine				**-**	**7.89 ± 0.05**	**-**	**-**	**12**
1		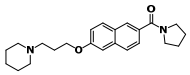		**-**	**8.29 ± 0.01**	**-**	**-**	**3**
12	**A**	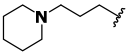	**-[d]**	**96.6 ± 0.33**	**7.33 ± 0.11**	**8.06 ± 0.06**	**0.74**	**5**
25	**B**	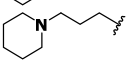	**-[d]**	**93.2 ± 0.29**	**6.42 ± 0.11[e]**	**7.04 ± 0.09**	**0.62**	**6**
17	**A**	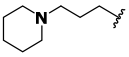	**4**	**88.2 ± 2.5**	**7.96 ± 0.06**	**7.36 ± 0.02**	**−0.59**	**3**
30	**B**	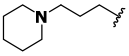	**4**	**88.9 ± 1.3**	**6.01 ± 0.13**	**6.69 ± 0.15**	**0.68**	**6**
16	**A**	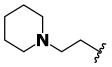	**4**	**86.6 ± 2.5**	**6.92 ± 0.12**	**6.56 ± 0.06**	**−0.36**	**5**
29	**B**	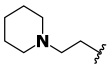	**4**	**91.3 ± 1.4**	**6.24 ± 0.02**	**5.96 ± 0.06**	**−0.28**	**3**
15	**A**	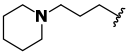	**3**	**95.4 ± 0.50**	**7.90 ± 0.07**	**7.26 ± 0.08**	**−0.63**	**5**
28	**B**	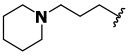	**3**	**86.8 ± 0.63**	**6.19 ± 0.11**	**7.32 ± 0.04**	**1.13**	**3**
14	**A**	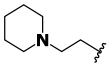	**3**	**90.6 ± 0.77**	**6.16 ± 0.06**	**5.85 ± 0.14**	**−0.30**	**4**
27	**B**	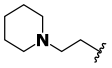	**3**	**89.3 ± 0.50**	**6.19 ± 0.02**	**6.38 ± 0.01**	**0.19**	**4**
13	**A**	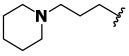	**2**	**88.9 ± 2.2**	**7.97 ± 0.13**	**7.55 ± 0.10**	**−0.41**	**4**
26	**B**	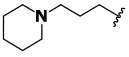	**2**	**88.4 ± 1.8**	**7.29 ± 0.08**	**7.09 ± 0.05**	**−0.19**	**4**
31	**A**	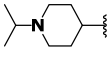	**3**	**90.5 ± 1.3**	**8.39 ± 0.09**	**7.40 ± 0.15**	**−0.98**	**5**
32	**A**	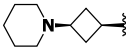	**3**	**96.8 ± 0.21**	**7.10 ± 0.12**	**6.48 ± 0.03**	**−0.62**	**3**
33	**A**	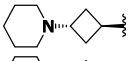	**3**	**94.6 ± 1.8**	**8.76 ± 0.09**	**7.71 ± 0.09**	**−1.05**	**4**
34	**B**	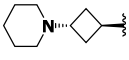	**3**	**89.3 ± 0.40**	**7.25 ± 0.04**	**7.15 ± 0.07**	**-0.10**	**4**

[a]Photostationary state area percentages after illumination at 10 mM in DMSO-d_6 and as determined by LCMS analysis at 254 nm. [b]Measured by displacement of [^{3}H]-N$^\alpha$-methylhistamine on HEK293T cell homogenates transiently expressing the H_3R. [c]Defined as pK_i PSS *cis* – pK_i *trans.* [d]Unsubstituted phenyl. [e]*Trans* sample contained 3.9 area % *cis* compound.

Binding mode characterization

Molecular modeling studies were performed for tool compounds **28** and **33** in order to gain insights into the molecular mechanism of the observed affinity changes upon isomerization. Molecular docking of **28** and **33** into a series of H_3R homology models yielded three potential binding modes in which the ligands form either an ionic interaction with the D114$^{3.32}$ or E205$^{5.46}$ residue in transmembrane helices (TM) 3 and 5, respectively[24,43,44]. The predicted binding modes share similarity with the binding orientation of ergotamine as observed in crystal structures of serotonin receptors 5-HT$_{1B}$ and 5-HT$_{2B}$ (PDB IDs: 4IAR, 4IB4)[45,46], aminergic GPCRs that share 54-62% sequence similarity for the binding site with H_3R (Fig. S22). Each of the 12 resulting H_3R-ligand complexes (2 ligands x 2 isomers x 3 binding modes) was investigated using 50 ns molecular dynamics (MD) simulations. The MD trajectories indicated that only for one binding mode (Fig. S22A) i) a consistent interaction fingerprint (IFP)[47] was observed throughout the simulation, and ii) the stable ligand binding mode was in line with the observed SAR data (Table 2). In this binding mode (Fig. 3C, D) the ligands form a stable salt bridge with D114$^{3.32}$ and move upward along TMs 2, 3, and 7 into the extracellular vestibule (ECV). The *trans* isomer of **33** adopts an elongated binding mode and makes multiple aromatic stacking interactions with Y91$^{2.61}$, Y94$^{2.64}$, Y394$^{7.35}$, and F398$^{7.39}$ while the carboxamide substituent is solvent exposed between the extracellular loops 1 and 2 (Fig. 3D). The *trans* isomer of **28**, on the other hand, adopts an arched binding mode within the extracellular vestibule (Fig. 3C) due to its *meta*-substitution. The binding modes of the *trans* isomers of both **28** and **33** are similar to the previously proposed binding modes for bitopic ligands of the aminergic dopamine D_2 receptor[48]. The *cis* isomers of both **28** and **33** adopt an almost identical binding mode (Fig. 3C, D) in which the carboxamide is buried in the ECV in close proximity to Y394$^{7.35}$, folded against the azobenzene, and located at the same position as the pyrrolidine moiety of ergotamine bound to 5-HT$_{1B}$ and 5-HT$_{2B}$ crystal structures (Fig. S23).

The opposite effects of *trans* to *cis* isomerization on the H_3R binding affinities of **28** and **33** can be explained by differences in: i) the complementarity of polar or apolar surface areas of the ligand and the protein binding site[49], and ii) the loss of conformational degrees of freedom as the result of ligand binding (conformer focusing[50]). Both isomers of **33** are expected to be less affected by conformer focusing due to their rigid cyclobutyl-spacer compared to the flexible propyl spacer of **28**. The decreased

affinity of the *trans* isomer versus the *cis* isomer of **28** (Table 2) can be explained by the fact that the apolar surface area of **28** is >4 times more solvent exposed in the *trans* isomer binding mode than in the *cis* isomer binding mode in H_3R. Conversely, the *trans* isomer of **33** has a reduced buried polar surface area compared to the folded *cis* isomer, while the apolar surface area of **33** is able to form a complementary fit with the apolar surface area of the H_3R binding site. In addition, the extended *trans* isomer of **33** allows more degrees of conformational freedom than the folded *cis* isomer, altogether resulting in an increased H_3R affinity for the *trans* isomer of **33** (Table 2).

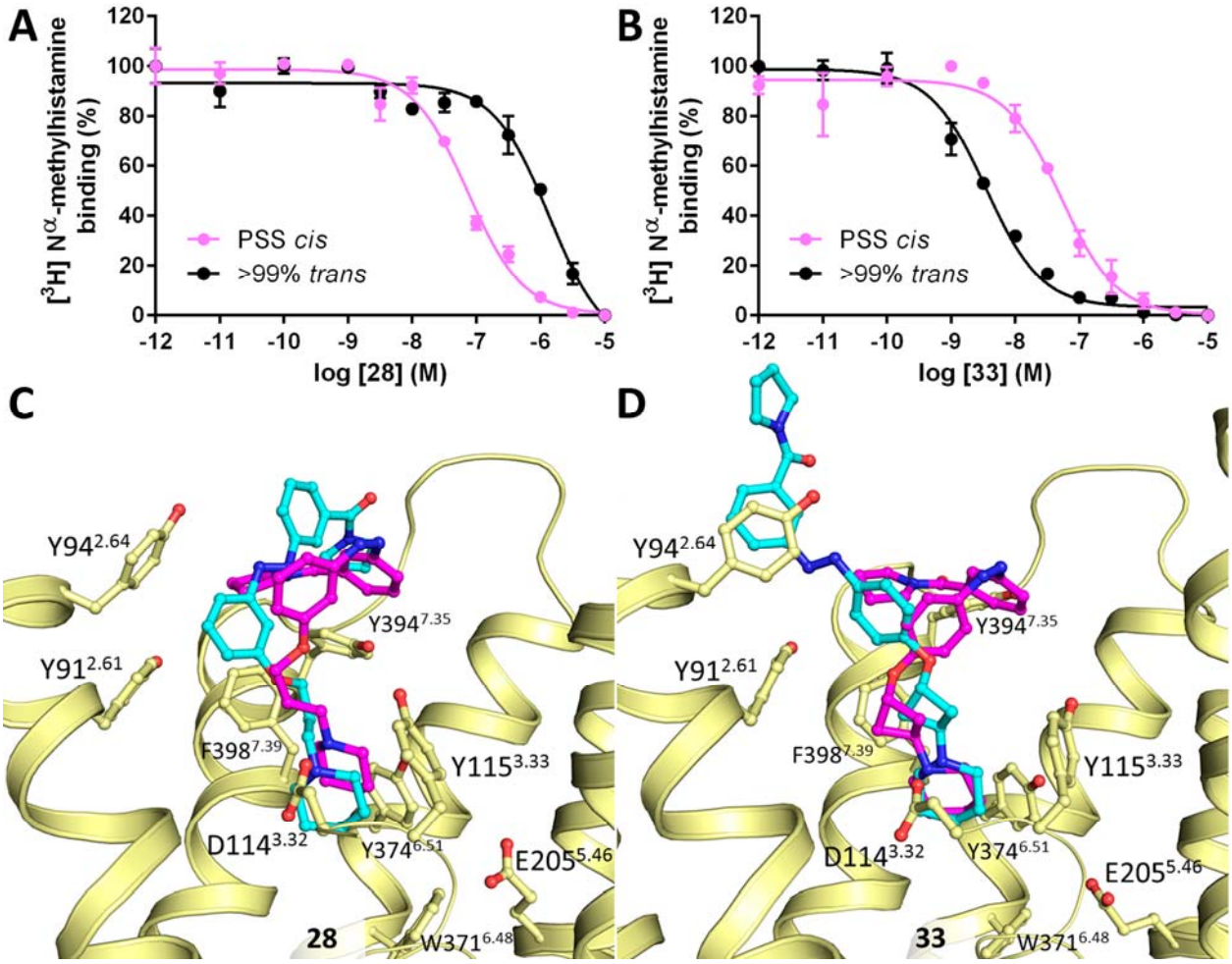

Figure 3: (A-B) Representative curves of [^{3}H]-N$^\alpha$-methylhistamine binding displacement by increasing concentrations (A) 28 or (B) 33. The curve indicated as PSS *cis* consists of predominantly (>90%) *cis* compound. (C-D) The proposed binding modes of (C) 28 and (D) 33 in an H_3R homology model based on representative MD snapshots. The cyan and magenta carbon atoms of the ligands correspond to the *trans* and *cis* isomer respectively and for clarity purposes parts of ECL1/TM3 and ECL2 are not shown.

Dynamic photochemical modulation of H_3R

As the new azobenzene-containing H_3R photoswitches can be dynamically and reversibly isomerized with light, we applied the two key H_3R photoswitches in a dynamic intact cell system with a real-time readout. Two-electrode voltage clamp (TEVC) using *Xenopus laevis* oocytes co-expressing H_3R and a GIRK channel composed of human GIRK1 (Kir3.1) and GIRK4 (Kir3.4) subunits (Fig. 4A)[51] allows for a real-time H_3R readout. In all experiments, H_3R-expressing oocytes were used that evoked a high current (>500 nA) upon histamine superfusion in 64 mM NaCl, 25 mM KCl, 15 mM HEPES, 0.8 mM $MgCl_2$ and 0.4 mM $CaCl_2$ pH 7.4 at a membrane potential of -80 mV. Under these conditions, histamine induced GIRK channel activation with a pEC_{50} value of 7.3 ± 0.06 (Fig. 4A). No currents were observed after histamine application to non-injected oocytes (Fig. S24). The GIRK channel activation by histamine (1 μM), could be fully inhibited upon simultaneous superfusion with the H_3R antagonist clobenpropit (1 μM) or by pretreating the oocytes with the $G\alpha_i$-protein inhibitor pertussis toxin (1.37 ng/oocyte) (Fig. S25 and S26). This shows that the histamine-induced current in *Xenopus laevis* oocytes co-expressing H_3R and a GIRK channel composed of human GIRK1 (Kir3.1) and GIRK4 (Kir3.4) subunits is H_3R mediated through $G\alpha_i$-protein coupling to GIRK.

We first ensured that photoisomerization behavior of **28** and **33** in HEPES pH 7.4 buffer was similar to behavior in 50 mM Tris-HCl pH 7.4 buffer (Fig. S4-S15). Next, we superfused *Xenopus* oocytes expressing H_3R and a GIRK channel with either *trans*-**28** or *trans*-**33** and histamine for dynamic receptor inhibition studies. Superfusion of only **28** or **33** on both non-injected and H_3R-GIRK expressing oocytes did not result in changes in current, confirming that these H_3R ligands act as antagonists (Fig S27 – S30). Illumination directly on the oocytes (Fig. 4A) in the absence of **28** or **33** did not change the magnitude of histamine evoked currents (Fig. S31). Yet, in the presence of either **33** or **28**, clear photoswitchable antagonism of the histamine-induced current was observed under alternating illumination. We confirmed that both compounds were able to show this behaviour in a concentration dependent fashion (Fig. S32, S33), yielding K_i values for **33** that nicely match the observed K_i values, obtained in the radioligand binding experiments (TEVC p*K*i >99% *trans*: 8.72 ± 0.11, PSS *cis*: 7.98 ± 0.15, radioligand binding: p*K*i >99% *trans*: 8.76 ± 0.09, PSS *cis*: 7.71 ± 0.09). An increase in histamine-induced GIRK activation was observed when *trans*-**33** was illuminated with 360 ± 25 nm, confirming that the H_3R antagonistic effect of **33** is reduced upon isomerization to its *cis* isomer. When subsequently the superfused oocytes were illuminated at 430 ± 17 nm, a decrease in H_3R-induced GIRK activation was observed due to a stronger H_3R antagonistic effect by the *trans* isomer of **33** as a consequence of

increased H_3R binding affinity. This effect could be repeated several times in subsequent illumination cycles in the same experiment (Fig. 4B). For **28**, the reciprocal light-induced H_3R affinity shift compared to **33** translated well to a reciprocal effect upon illumination in the TEVC setup (Fig. 4C). That is, **28** reached the highest H_3R inhibition, measured as reduced histamine-induced GIRK channel activation, upon illumination with 360 ± 25 nm. Also, **28** could be effectively switched back in the TEVC setup upon illumination with 430 ± 17 nm, and again the GPCR blocking properties could be modulated by alternating illumination (Fig. 4C). These experiments demonstrate the rapid bi-directional modulation of the H_3R using the two complementary photoswitchable ligands **28** and **33**.

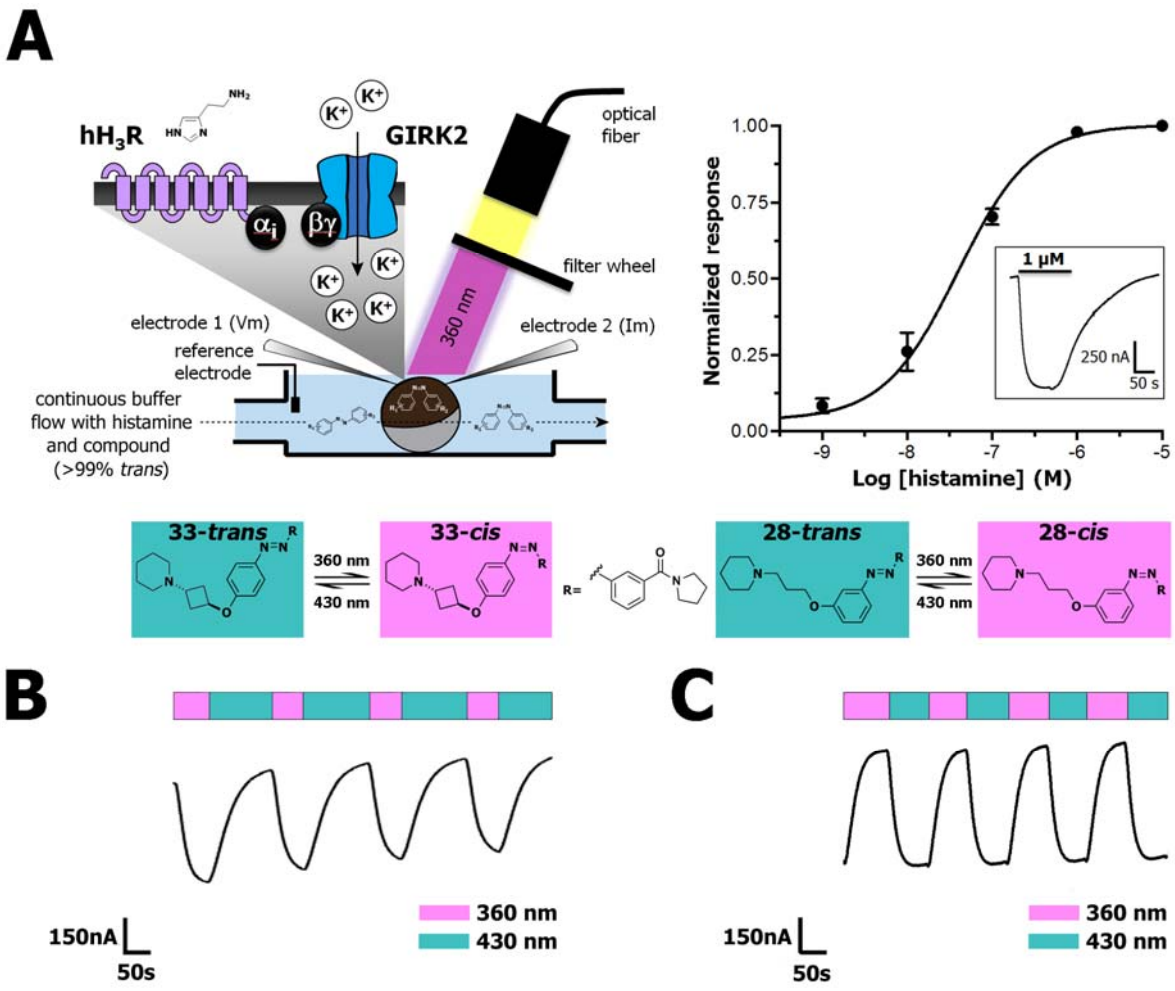

Figure 4: (A) Schematic drawing of the TEVC setup used for dynamic H_3R and GIRK current (in)activation and concentration-response curve of histamine evoked currents in *Xenopus* oocytes expressing H_3R and GIRK. The insert shows the current increase upon continuous histamine (1 µM) perfusion in time. (B) Representative part of a GIRK-mediated current trace during continuous perfusion with 5 µM histamine in competition with 1 µM 33 under illumination of the *Xenopus* oocyte with alternating 360 ± 25 and 430 ± 17 nm wavelength as measured by TEVC. An extended time trace is available in Figure

S34. (C) Representative part of a GIRK mediated current trace during continuous perfusion with 5 μM histamine in competition with 1 μM 28 and illumination of the oocyte with alternating 360 ± 25 and 430 ± 17 nm wavelength as measured by TEVC. An extended time trace is available in Figure S35.

Conclusions

A robust bi-directional photochemical toolbox for dynamic antagonism of the H_3R has been successfully developed, using a core-centered approach replacing a naphthalene moiety in a known scaffold by a properly substituted azobenzene unit. SAR exploration delivered 16 compounds that show a shift in binding affinity for the H_3R upon photoisomerization. Two key compounds, **28** and **33**, were selected based on their 13.5-fold increase or 11.2-fold decrease in H_3R binding affinity upon photoisomerization, respectively. The long thermal relaxation half-lives and resistance to fatigue of these compounds allowed in-depth spectroscopic analysis (NMR, LC-MS, UV-Vis) of the photochemical properties. The rapid photochemical isomerization directly translated to dynamic, light-modulated H_3R blockade in real-time electrophysiology experiments using H_3R and GIRK co-expressing *Xenopus* oocytes. In this dynamic experimental setup, histamine-induced GPCR activation could be modulated on a time scale of seconds and we were able to show real-time, light-sensitive blockade of the H_3R activation by both new tool compounds. In our view **28** (VUF14738) and **33** (VUF14862) are highly useful photopharmacological tools for temporal studies to dissect the complex signaling cascade of H_3R. Moreover, the presented bi-directional modulation of H_3R protein by closely related photosensitive analogs of the same core scaffold further emphasizes the exceptional opportunities of conformational modulation of the GPCR protein family.

Experimental section

Synthesis and characterization of compounds

All starting materials were obtained from commercial suppliers (primarily being Sigma-Aldrich, Acros Organics, Fluorochem and Strem Chemicals) and used without purification. 4-hydroxyazobenzene (**8**) was obtained from Sigma-Aldrich**.** *Cis*-3-piperidin-1-ylcyclobutanol (**35**) was synthesized according to the literature procedure of Wijtmans *et al*.[52]. Anhydrous THF and DCM were obtained by passing it through an activated alumina column prior to use. Anhydrous toluene was freshly distilled over CaH_2, or dried over activated 4Å molecular sieves, which were added at least 24 hrs before use. Anhydrous DMF was purchased from Acros Organics (Geel, Belgium) and used without prior purification. All reactions were carried out under nitrogen atmosphere unless mentioned otherwise. TLC analyses were performed using Merck F254 aluminum-backed silica plates and visualized 254 nm UV-light or a potassium permanganate stain. Flash column chromatography was executed using Silicycle Siliaflash F60 silica gel, or by means of a Biotage® Isolera equipment using Biotage® SNAP columns. All HRMS spectra were recorded on a Bruker micrOTOF mass spectrometer using ESI in positive ion mode. All NMR spectra were recorded on either a Bruker Avance 250, Bruker Avance 400, Bruker Avance 500 or Bruker Avance 600 spectrometer. The peak multiplicities are defined as follows: s, singlet; d, doublet; t, triplet; q, quartet; p, pentet; dd, doublet of doublets; dt, doublet of triplets; td, triplet of doublets; bs, broad singlet; m, multiplet. The spectra were referenced to the internal solvent peak as follows: $CDCl_3$ (^1H = 7.26 ppm, ^{13}C = 77.16 ppm), DMSO-d_6 (^1H = 2.50 ppm, ^{13}C = 39.52 ppm), CD_3OD (^1H = 3.31 ppm, ^{13}C = 49.00 ppm)[53]. IUPAC names were adapted from ChemBioDraw Ultra 14.0 (Perkin-Elmer). Purities were measured with the aid of analytical LC-MS using a Shimadzu LC-20AD liquid chromatography pump system with a Shimadzu SPDM20A diode array detector with the MS detection performed with a Shimadzu LCMS-2010EV mass spectrometer operating in both positive and negative ionization mode. The column used was an Xbridge (C18) 5 µm column (50 mm × 4.6 mm or 100 mm × 4.6 mm). The following solutions are used for the eluents. Solvent A: water: formic acid 999:1 and solvent B: acetonitrile: formic acid 999:1. The eluent program used is as follows: flow rate: 1.0 mL/min, start 95% A in a linear gradient to 10% A over 4.5 min, hold 1.5 min at 10% A, in 0.5 min in a linear gradient to 95% A, hold 1.5 min at 95% A, total runtime: 8.0 min. Compound purities were calculated as the percentage peak area of the analyzed compound by UV detection at 254 nm. All chemistry and analyses of photosensitive compounds were carried out under dimmed or red light.

Detailed chemical experimental procedures and chemical analyses are supplied in the Supporting Information.

Photochemistry

UV-Vis spectra were obtained using a Thermo-scientific Evolution 201 PC spectrophotometer or a Shimadzu UV-2401 PC spectrophotometer. Fits of UV-Vis spectroscopy data were generated using Mathworks Matlab R2014A (8.3.0.532). Illumination was executed using a Sutter instruments Lambda LS with a 300 Watt full-spectrum lamp connected to a Sutter instruments Lambda 10-3 optical filter changer equipped with 430 ± 17 nm and 360 ± 25 nm filters. For photochemical analyses illuminations were performed in Hellma Suprasil™ quartz 114-QS cuvettes. Thermal relaxation experiments and Arrhenius extrapolations were performed according to Priimagi et al.[34] using a compound concentration of 25 µM in 50 mM Tris-HCl pH 7.4 buffer + 1% DMSO-d_6 and temperatures of 60 °C, 70 °C and 80 °C. Illuminations for pharmacological experiments were performed in cylindrical clear glass vials with a volume of 4.5 mL. The typical distance between light source and vial or cuvette was 2 cm. In illuminations during TVEC experiments the light-source was positioned at 5 cm from the chamber containing the

oocyte. The focused beam of the light source has a diameter of 1.8 cm and the beam was pointed such that it illuminated the full oocyte. The light intensity on the oocyte is 0.77 mW/mm^2 using the 360 ± 25 nm filter and 0.57 mW/mm^2 for the 430 ± 17 nm filter as measured using a Thorlabs PM16-401 power meter.

Computational chemistry

Homology model construction. The sequence of H_3R was obtained from UniProt (accession code Q9Y5N1) and aligned to the unique sequences of crystallized aminergic GPCRs (PDB accessed at 3 Nov. 2015). The sequence similarity and identity were assessed for the full sequence, each TM helix, extracellular loop 2, and the binding pocket as previously defined[23]. Based on this analysis the sequence alignment of H_3R to H_1R, M_3R, D_3R, 5-$HT_{1B}R$ and 5-$HT_{2B}R$ and their crystal structures (PDB-codes 3RZE, 4U15, 3PBL, 4IAR, 4IB4) was used as input for MODELLER (version 9.15)[54]. 500 different homology models were constructed from which 36 were selected based on visual inspection. Compounds *trans*-**28**, *cis*-**28**, *trans*-**33**, and *cis*-**33** were subsequently docked into each model using PLANTS[55] (settings: speed 1, scoring function ChemPLP, 10-fold docking, 50 proposed poses per fold) into each of the models while treating the side chains of E206$^{5.46}$ and F398$^{7.39}$ as flexible. The resulting 26,000 docking poses were filtered using IFP[47] on either and ionic and H-bond interaction with D114$^{3.32}$ or E206$^{5.46}$ from which the top 5 ChemPLP-scored poses were kept for further processing yielding 396 H_3R-ligand complexes. Visual inspection highlighted 3 clusters of potential binding modes. From each ligand in each binding mode cluster one model was selected for further investigation with molecular dynamics simulations.

Molecular dynamics simulations. Each ligand-H_3R complex was aligned to the membrane-aligned H_1R structure from the OPM database. A sodium ion was added in the sodium binding site based on high-resolution sodium-bound β_1-adrenoceptor crystal structure (PDB-code 4BVN). Subsequently the rotamers from the sodium binding site residues were manually optimized[56]. The H_3R-ligand complexes were embedded in a pre-equilibrated box containing a lipid bilayer (134 POPC lipids), explicit solvent (~11,000 water molecules) and a 0.15 M concentration of NaCl (~70 ions). Using MOE (v2015.1001; Chemical Computing Group Inc., Montreal, Quebec, Canada) the ligand-H_3R complex was solvated, and waters between the receptor and the membrane and outside the receptor were removed. The ligands were parameterized for GAFF using Amber's antechamber with AM1-BCC partial charges. The resulting parameters of the ligand were checked, and the azobenzene parameters were optimized in line with the parameters reported by Schäfer et al.[57]. The AMBER99SB*-ILDN force field was used for the protein and the lipids and waters were described according to the Berger lipid parameters and the TIP3P model, respectively[58]. After neutralizing the system, a 1000-step steepest descent minimization of the system was performed and after which the complex was equilibrated for 75 and 300 ps using a 1 and 2 fs time step, respectively. A subsequent production run of 50 ns as an NVT ensemble was performed for each combination. The trajectories were analyzed using IFP[47] resulting in a time-based interaction profile for each H_3R-ligand complex. These MD simulations were performed using GROMACS 5.1[59].

Pharmacology

General. Within this paper, the 445-isoform of the human H_3R is referred to as wild-type receptor. [^{3}H]-Mepyramine (specific activity 20 Ci/mmol^{-1}), [^{125}I]-Iodoaminopotentidine (specific activity 2200 Ci/mmol^{-1}), [^{3}H]-N$^{\alpha}$-methylhistamine (specific activity 78.3 Ci/mmol^{-1}) and [^{3}H]-histamine (specific activity 17.5 Ci/mmol^{-1}) were purchased from PerkinElmer (Groningen, the Netherlands). All other chemicals were of analytical grade and obtained from commercial sources.

Cell culture & transfection. Human embryonic kidney 293T cells (HEK293T cells) were cultured in Dulbecco's modified eagle medium (DMEM) supplemented with 10% fetal bovine serum (FBS), penicillin (50 IU/mL) and streptomycin (50 μg/mL). HEK293T cells were transiently transfected with H_3R cDNA using the polyethylenimine (PEI) method. In brief, 24 hrs prior to transfection $2 \cdot 10^6$ cells were seeded on a 10 cm dish. Cells were transfected with 5 μg H_3R cDNA and 20 μg PEI in 500 μL 150 mM NaCl-solution. DNA-PEI mixture was incubated for 15-30 min at 22 °C before dropwise addition to the cells. Cells were maintained for 48 hrs at 37 °C with 5% CO_2 before harvesting.

Preparation of cell homogenates. 48 hrs after transfection cells were detached and collected from the plates by vigorous pipetting using phosphate buffered saline (PBS). Cells were centrifuged at 3000 rpm for 10 min and cell-pellet was stored at -20 °C until the day of experiment.

Radioligand binding assay. For radioligand binding experiments samples were pretreated to obtain *trans* and *cis* samples. In brief, 1 mM ligand solution was divided in two samples which were either illuminated at 360 ± 25 nm until their photostationary state was reached as analyzed by LC-MS, or kept in the dark for the same duration as the illuminated samples. All subsequent handling was performed in the dark or under near-infrared light. [^{3}H]-N$^\alpha$-methylhistamine binding assays were performed in a total volume of 100 μl consisting of cold ligand (increasing concentration ranging from 10^{-5} M to 10^{-12} M) prepared in assay buffer [50 mM Tris-HCl pH 7.4], 1.6 nM [^{3}H]-N$^\alpha$-methylhistamine and HEK293T cell homogenates transiently expressing the human H_3R (>25 μg/50 μl). The mixture was incubated for 2 hrs at 22 °C before termination by rapid filtration over a 96 well GF/C filter plate pre-coated with 0.5% PEI using Perkin Elmer 96-well filtermate-harvester (Perkin Elmer). The filter was washed 5 times with ice-cold wash buffer [50mM Tris-HCl pH 7.4, 4 °C]. 5 hrs after addition of Microscint O scintillation liquid filter-bound radioactivity was measured using a microbeta wallac trilux scintillation counter (Perkin Elmer).

Binding selectivity screening. H_1R radioligand binding assays were performed according to Kuhne *et al.*[60] using an incubation time of 2 hours instead of 4 hours. H_2R radioligand binding assays were performed according to Leurs *et al*.[61] using HEK293T cells instead of CHO cells and a total volume of 400 μL instead of 200 μL. H_4R radioligand binding assays were performed according to Nijmeijer *et al*.[62]

Data analysis. All experiments were analyzed using Graphpad prism 6.05 (Graphpad software inc., San Diego, USA) IC_{50} values obtained from competition binding experiments were converted to K_i values using the Cheng-Prusoff equation[63].

Two electrode voltage clamp (TEVC) assay

RNA synthesis. The Kir3.1 and Kir3.4 were both supplied in the pcDNA3.1 vector and were a kind gift of K. Sahlholm (Karolinska Institute, Stockholm, Sweden). The H_3R was cloned into the pCIneo vector. Restriction enzymes BAMHI and NdeI were used to linearize the constructs pCIneo-H_3R and pcDNA3.1-Kir3.1 and 3.4, respectively. After the digestion, 0.5% SDS and Proteinase K (200 μg/mL) were added and the mixture was incubated at 50 ^{o}C for 30 min. DNA was extracted by phenol/chloroform and the precipitation method. The quality and digestion was checked on 1% agarose gel. The cRNA synthesis was performed with the T7 mMessage mMachine kit (Ambion, Austin, TX, USA). After the synthesis, the cRNA quality and amount was checked on a denaturating gel for RNA as described by Almeida *et al*.[64].

H_3R and GIRK expression in oocytes. Xenopus laevis oocytes were supplied as "topgrade" oocytes (Ecocyte, Castrop-Rauxel, Germany). Each oocyte was injected with a volume of 46 nL, containing 3 ng cRNA of each GIRK subunit and 50 ng cRNA of the H_3R or with 46 nL of RNAse free water as control with the Nanoject II (Drummond Scientific Company, Broomall, PA, USA). The oocytes were incubated for 4-6 days at 12 °C in modified Barth solution (88 mM NaCl, 1 mM KCl, 2.4 mM $NaHCO_3$, 15 mM

HEPES, 0.33 mM $Ca(NO_3)_2$, 0.41 mM $CaCl_2$, 0.82 mM $MgSO_4$, 2.5 mg pyruvic acid, 100 μg/mL Streptomycin, 50 μg/mL Gentamycin, adjusted with Tris to pH 7.4), as described by Sahlholm *et al*.[51].

Two-electrode voltage clamp. Two-electrode voltage clamp (TEVC) was performed with the Axoclamp 900A amplifier and the Digidata 1550 Digitizer. The currents were recorded and analyzed with pClamp 10.6 (Molecular Devices, Sunnyvale, CA, USA). Glass micropipettes were pulled from borosilicate capillaries (GC150-10, Harvard Apparatus, Edenbridge, UK) with the P-1000 micropipette puller (Sutter Instrument, Novato, CA, USA,), to have a resistance of 1-3 MΩ when filled with 3 M KCl solution. The oocyte was positioned in the recording chamber (RC-1Z, Warner Instruments, Hamden, CT, USA) and by gravity flow, high potassium solution (64 mM NaCl, 25 mM KCl, 0.8 mM $MgCl_2$, 0.4 mM $CaCl_2$, 15 mM HEPES and adjusted with Bis-Tris Propane to pH 7.4) was perfused through the recording chamber. For the study of H_3R ligands, the membrane potential was clamped at -80 mV and the evoked currents were measured at room temperature (~20 °C). The ligands (histamine, clobenpropit, **28** and **33**) were diluted, in the high potassium solution to obtain the appropriate concentrations. For the photoswitchable ligands (**28** and **33**), the TEVC was performed in the dark and the different wavelengths (360 ± 25 nm and 430 ± 17 nm) were applied directly on the oocyte in the recording chamber for 1 min (with **28**) or 2 min (with **33**) with a Sutter instruments Lambda LS with a 300 watt full spectrum lamp connected to a Sutter instruments Lambda 10-3 optical filter changer equipped with 430 ± 17 nm and 360 ± 25 nm filters to observe the (functional) switch of the ligands. For the Pertussis toxin experiment, 46 nL (1.38 ng) of PTX or water as control was injected in H_3R/GIRK expressing oocytes (4-6 days after cRNA injection) with the Nanoject II The oocytes were incubated for another 7 hrs before measuring the currents evoked by 1 μM histamine to the oocytes.

Associated content

Detailed synthetic procedures, chemical analyses and spectra, and additional data as noted in text.

Acknowledgements

All authors acknowledge the Netherlands Organisation for Scientific Research (NWO) for financial support (TOPPUNT, “7 ways to 7TMR modulation (7-to-7)”, 718.014.002). EWEV is supported by NWO ECHO project 711.013.014. All authors participate in the European Cooperation in Science and Technology Action CM1207 [GPCR-Ligand Interactions, Structures, and Transmembrane Signaling: A European Research Network (GLISTEN)]. We thank Hans Custers for HRMS analyses, Yara Huppelschoten for determining the selectivity of the key compounds amongst the histamine receptor family, and Andrea Van de Stolpe and Ken Lion for setting up the photochemical equipment. Kristoffer Sahlholm (Karolinska institute) is kindly acknowledged for providing the pcDNA3.1-Kir3.1 and -Kir3.4 plasmids.

Competing financial interests

The authors declare no competing financial interests.

References

(1) Broichhagen, J.; Frank, J. A.; Trauner, D. *Acc. Chem. Res.* **2015**, *48*, 1947.

(2) Lerch, M. M.; Hansen, M. J.; van Dam, G. M.; Szymanski, W.; Feringa, B. L. *Angew. Chem. Int. Ed. Engl.* **2016**, *55*, 10978

(3) Szobota, S.; Isacoff, E. Y. *Annu. Rev. Biophys.* **2010**, *39*, 329.

(4) Beharry, A. A.; Woolley, G. A. *Chem. Soc. Rev.* **2011**, *40*, 4422.

(5) Szymanski, W.; Beierle, J. M.; Kistemaker, H. A.; Velema, W. A.; Feringa, B. L. *Chem. Rev.* **2013**, *113*, 6114.

(6) Velema, W. A.; Szymanski, W.; Feringa, B. L. *J Am Chem Soc* **2014**, *136*, 2178.

(7) Stein, M.; Middendorp, S. J.; Carta, V.; Pejo, E.; Raines, D. E.; Forman, S. A.; Sigel, E.; Trauner, D. *Angew. Chem. Int. Ed. Engl.* **2012**, *51*, 10500.

(8) Frank, J. A.; Moroni, M.; Moshourab, R.; Sumser, M.; Lewin, G. R.; Trauner, D. *Nat. Commun.* **2015**, *6*, 7118.

(9) Broichhagen, J.; Schonberger, M.; Cork, S. C.; Frank, J. A.; Marchetti, P.; Bugliani, M.; Shapiro, A. M.; Trapp, S.; Rutter, G. A.; Hodson, D. J.; Trauner, D. *Nat. Commun.* **2014**, *5*, 5116.

(10) Pittolo, S.; Gomez-Santacana, X.; Eckelt, K.; Rovira, X.; Dalton, J.; Goudet, C.; Pin, J. P.; Llobet, A.; Giraldo, J.; Llebaria, A.; Gorostiza, P. *Nat. Chem. Biol.* **2014**, *10*, 813.

(11) Schönberger, M.; Trauner, D. *Angew. Chem. Int. Ed. Engl.* **2014**, *53*, 3264.

(12) Bahamonde, M. I.; Taura, J.; Paoletta, S.; Gakh, A. A.; Chakraborty, S.; Hernando, J.; Fernandez-Duenas, V.; Jacobson, K. A.; Gorostiza, P.; Ciruela, F. *Bioconjug. Chem.* **2014**, *25*, 1847.

(13) Broichhagen, J.; Johnston, N. R.; von Ohlen, Y.; Meyer-Berg, H.; Jones, B. J.; Bloom, S. R.; Rutter, G. A.; Trauner, D.; Hodson, D. J. *Angew. Chem. Int. Ed. Engl.* **2016**, *55*, 5865.

(14) Westphal, M.; Schafroth, M. A.; Sarott, R.; Imhof, M.; Bold, C.; Leippe, P.; Dhopeshwarkar, A.; Grandner, J.; Katritch, V.; Mackie, K.; Trauner, D.; Carreira, E. M.; Frank, J. A. *J Am Chem Soc* **2017**.

(15) Haas, H.; Panula, P. *Nat. Rev. Neurosci.* **2003**, *4*, 121.

(16) Leurs, R.; Bakker, R. A.; Timmerman, H.; de Esch, I. J. P. *Nat. Rev. Drug. Discov.* **2005**, *4*, 107.

(17) Panula, P.; Chazot, P. L.; Cowart, M.; Gutzmer, R.; Leurs, R.; Liu, W. L.; Stark, H.; Thurmond, R. L.; Haas, H. L. *Pharmacol. Rev.* **2015**, *67*, 601.

(18) Schwartz, J. C. *Brit. J. Pharmacol.* **2011**, *163*, 713.

(19) Lebois, E. P.; Jones, C. K.; Lindsley, C. W. *Curr. Top. Med. Chem.* **2011**, *11*, 648.

(20) Leurs, R.; Vischer, H. F.; Wijtmans, M.; de Esch, I. J. P. *Trends Pharmacol. Sci.* **2011**, *32*, 250.

(21) Celanire, S.; Wijtmans, M.; Talaga, P.; Leurs, R.; de Esch, I. J. *Drug Discov Today* **2005**, *10*, 1613.

(22) Uveges, A. J.; Kowal, D.; Zhang, Y.; Spangler, T. B.; Dunlop, J.; Semus, S.; Jones, P. G. *J. Pharmacol. Exp. Ther.* **2002**, *301*, 451.

(23) Kooistra, A. J.; Kuhne, S.; de Esch, I. J.; Leurs, R.; de Graaf, C. *Br. J. Pharmacol.* **2013**, *170*, 101.

(24) Axe, F. U.; Bembenek, S. D.; Szalma, S. *J. Mol. Graph. Model.* **2006**, *24*, 456.

(25) Lorenzi, S.; Mor, M.; Bordi, F.; Rivara, S.; Rivara, M.; Morini, G.; Bertoni, S.; Ballabeni, V.; Barocelli, E.; Plazzi, P. V. *Bioorg. Med. Chem.* **2005**, *13*, 5647.

(26) Kim, S.-K.; Fristrup, P.; Abrol, R.; Goddard, W. A. *J. Chem. Inf. Model.* **2011**, *51*, 3262.

(27) Sander, K.; von Coburg, Y.; Camelin, J. C.; Ligneau, X.; Rau, O.; Schubert-Zsilavecz, M.; Schwartz, J. C.; Stark, H. *Bioorg Med Chem Lett* **2010**, *20*, 1581.

(28) Roche, O.; Nettekoven, M.; Vifian, W.; Sarmiento, R. M. *Bioorg. Med. Chem. Lett.* **2008**, *18*, 4377.

(29) Arrang, J. M.; Garbarg, M.; Lancelot, J. C.; Lecomte, J. M.; Pollard, H.; Robba, M.; Schunack, W.; Schwartz, J. C. *Nature* **1987**, *327*, 117.

(30) Alves-Rodrigues, A.; Leurs, R.; Wu, T. S.; Prell, G. D.; Foged, C.; Timmerman, H. *Br J Pharmacol* **1996**, *118*, 2045.

(31) Nieto-Alamilla, G.; Marquez-Gomez, R.; Garcia-Galvez, A. M.; Morales-Figueroa, G. E.; Arias-Montano, J. A. *Mol Pharmacol* **2016**, *90*, 649.

(32) Wu, X.; Fors, B. P.; Buchwald, S. L. *Angew. Chem. Int. Ed. Engl.* **2011**, *50*, 9943.

(33) Wijtmans, M.; Denonne, F.; Celanire, S.; Gillard, M.; Hulscher, S.; Delaunoy, C.; Van Houtvin, N.; Bakker, R. A.; Defays, S.; Gerard, J.; Grooters, L.; Hubert, D.; Timmerman, H.; Leurs, R.; Talaga, P.; de Esch, I. J. P.; Provins, L. *Medchemcomm* **2010**, *1*, 39.

(34) Ahmed, Z.; Siiskonen, A.; Virkki, M.; Priimagi, A. *Chem Commun* **2017**, *53*, 12520.

(35) Bleger, D.; Hecht, S. *Angew. Chem. Int. Ed. Engl.* **2015**, *54*, 11338.

(36) Dong, M.; Babalhavaeji, A.; Hansen, M. J.; Kalman, L.; Woolley, G. A. *Chem. Commun. (Camb)* **2015**, *51*, 12981.

(37) Talaty, E. R.; Fargo, J. C. *Chem Commun* **1967**, 65.

(38) Garcia-Amoros, J.; Velasco, D. *Beilstein J Org Chem* **2012**, *8*, 1003.
(39) Asano, T.; Okada, T.; Shinkai, S.; Shigematsu, K.; Kusano, Y.; Manabe, O. *Journal of the American Chemical Society* **1981**, *103*, 5161.
(40) Serra, F.; Terentjev, E. M. *Macromolecules* **2008**, *41*, 981.
(41) Whitten, D. G.; Wildes, P. D.; Pacifici, J. G.; Irick, G. *J. Am. Chem. Soc.* **1971**, *93*, 2004.
(42) Dvorak, C. A.; Apodaca, R.; Barbier, A. J.; Berridge, C. W.; Wilson, S. J.; Boggs, J. D.; Xiao, W.; Lovenberg, T. W.; Carruthers, N. I. *J. Med. Chem.* **2005**, *48*, 2229.
(43) Rai, B. K.; Tawa, G. J.; Katz, A. H.; Humblet, C. *Proteins* **2010**, *78*, 457.
(44) Levoin, N.; Labeeuw, O.; Krief, S.; Calmels, T.; Poupardin-Olivier, O.; Berrebi-Bertrand, I.; Lecomte, J. M.; Schwartz, J. C.; Capet, M. *Bioorg. Med. Chem.* **2013**, *21*, 4526.
(45) Wang, C.; Jiang, Y.; Ma, J.; Wu, H.; Wacker, D.; Katritch, V.; Han, G. W.; Liu, W.; Huang, X. P.; Vardy, E.; McCorvy, J. D.; Gao, X.; Zhou, X. E.; Melcher, K.; Zhang, C.; Bai, F.; Yang, H.; Yang, L.; Jiang, H.; Roth, B. L.; Cherezov, V.; Stevens, R. C.; Xu, H. E. *Science* **2013**, *340*, 610.
(46) Wacker, D.; Wang, C.; Katritch, V.; Han, G. W.; Huang, X. P.; Vardy, E.; McCorvy, J. D.; Jiang, Y.; Chu, M.; Siu, F. Y.; Liu, W.; Xu, H. E.; Cherezov, V.; Roth, B. L.; Stevens, R. C. *Science* **2013**, *340*, 615.
(47) Marcou, G.; Rognan, D. *J. Chem. Inf. Model.* **2007**, *47*, 195.
(48) Lane, J. R.; Donthamsetti, P.; Shonberg, J.; Draper-Joyce, C. J.; Dentry, S.; Michino, M.; Shi, L.; Lopez, L.; Scammells, P. J.; Capuano, B.; Sexton, P. M.; Javitch, J. A.; Christopoulos, A. *Nat. Chem. Biol.* **2014**, *10*, 745.
(49) Schmidtke, P.; Luque, F. J.; Murray, J. B.; Barril, X. *J. Am. Chem. Soc.* **2011**, *133*, 18903.
(50) Tirado-Rives, J.; Jorgensen, W. L. *J. Med. Chem.* **2006**, *49*, 5880.
(51) Sahlholm, K.; Nilsson, J.; Marcellino, D.; Fuxe, K.; Arhem, P. *Eur. J. Pharmacol.* **2007**, *567*, 206.
(52) Wijtmans, M.; Denonne, F.; Célanire, S.; Gillard, M.; Hulscher, S.; Delaunoy, C.; Van houtvin, N.; Bakker, R. A.; Defays, S.; Gérard, J.; Grooters, L.; Hubert, D.; Timmerman, H.; Leurs, R.; Talaga, P.; de Esch, I.; Provins, L. *Med. Chem. Commun.* **2010**, *1*, 39.
(53) Fulmer, G. R.; Miller, A. J. M.; Sherden, N. H.; Gottlieb, H. E.; Nudelman, A.; Stoltz, B. M.; Bercaw, J. E.; Goldberg, K. I. *Organometallics* **2010**, *29*, 2176.
(54) Sali, A.; Blundell, T. L. *J. Mol. Biol.* **1993**, *234*, 779.
(55) Korb, O.; Stutzle, T.; Exner, T. E. *J. Chem. Inf. Model.* **2009**, *49*, 84.
(56) Miller-Gallacher, J. L.; Nehme, R.; Warne, T.; Edwards, P. C.; Schertler, G. F.; Leslie, A. G.; Tate, C. G. *PLoS One* **2014**, *9*, e92727.
(57) Schäfer, L. V.; Muller, E. M.; Gaub, H. E.; Grubmuller, H. *Angew. Chem. Int. Ed. Engl.* **2007**, *46*, 2232.
(58) Cordomi, A.; Caltabiano, G.; Pardo, L. *J. Chem. Theory Comput.* **2012**, *8*, 948.
(59) Berendsen, H. J. C.; van der Spoel, D.; van Drunen, R. *Comput. Phys. Commun.* **1995**, *91*, 43.
(60) Kuhne, S.; Kooistra, A. J.; Bosma, R.; Bortolato, A.; Wijtmans, M.; Vischer, H. F.; Mason, J. S.; de Graaf, C.; de Esch, I. J.; Leurs, R. *J Med Chem* **2016**, *59*, 9047.
(61) Leurs, R.; Smit, M. J.; Menge, W. M.; Timmerman, H. *Br J Pharmacol* **1994**, *112*, 847.
(62) Nijmeijer, S.; Vischer, H. F.; Rosethorne, E. M.; Charlton, S. J.; Leurs, R. *Mol Pharmacol* **2012**, *82*, 1174.
(63) Yung-Chi, C.; Prusoff, W. H. *Biochem. Pharmacol.* **1973**, *22*, 3099.
(64) Almeida, P.; de Boer, G.-J.; de Boer, A. H. *J. Plant Physiol.* **2014**, *171*, 438.

Graphical abstract